Histidine[118] in the S2–S3 Linker Specifically Controls Activation of the KAT1 Channel Expressed in *Xenopus* Oocytes

Xiang D. Tang*, Irene Marten†, Petra Dietrich‡, Natalya Ivashikina‡, Rainer Hedrich‡, and Toshinori Hoshi*
*Department of Physiology and Biophysics, The University of Iowa, Iowa City, Iowa 52242, USA, †Institut für Biophysik, Universität Hannover, Herrenhäuserstr. 2, D-30419 Hannover, Germany, and ‡Julius-von-Sachs-Institut, Molekulare Pflanzenphysiologie und Biophysik, Lehrstuhl Botanik I, Universität Würzburg, Julius-von-Sachs-Platz 2, D-97082 Würzburg, Germany

ABSTRACT The guard cell K^+ channel KAT1, cloned from *Arabidopsis thaliana*, is activated by hyperpolarization and regulated by a variety of physiological factors. Low internal pH accelerated the activation kinetics of the KAT1 channel expressed in *Xenopus* oocytes with a pK of approximately 6, similar to guard cells in vivo. Mutations of histidine-118 located in the putative cytoplasmic linker between the S2 and S3 segments profoundly affected the gating behavior and pH dependence. At pH 7.2, substitution with a negatively charged amino acid (glutamate, aspartate) specifically slowed the activation time course, whereas that with a positively charged amino acid (lysine, arginine) accelerated. These mutations did not alter the channel's deactivation time course or the gating behavior after the first opening. Introducing an uncharged amino acid (alanine, asparagine) at position 118 did not have any obvious effect on the activation kinetics at pH 7.2. The charged substitutions markedly decreased the sensitivity of the KAT1 channel to internal pH in the physiological range. We propose a linear kinetic scheme to account for the KAT1 activation time course at the voltages where the opening transitions dominate. Changes in one forward rate constant in the model adequately account for the effects of the mutations at position 118 in the S2–S3 linker segment. These results provide a molecular and biophysical basis for the diversity in the activation kinetics of inward rectifiers among different plant species.

INTRODUCTION

Plants carry out photosynthesis to convert CO_2 and water into carbohydrates and O_2. To efficiently perform these vital photochemical and biochemical reactions, stomatal valves in the epidermis of plant leaves must be able to open and close to optimize the uptake of CO_2 and the loss of water vapor. Various species of plants differ in their stomatal movement kinetics, which are modulated by environmental conditions and plant growth regulators, such as light, CO_2, phytohormones, pH, and Ca^{2+} (Raschke, 1979).

K^+ ion fluxes across the guard-cell plasma membrane play an essential role in stomatal movement (Fischer, 1968). Two types of K^+ channels, hyperpolarization-activated K^+ channels (K_H, K_{in} or inward-rectifying K^+ channels [IRC]) and depolarization-activated K^+ channels (K_D, K_{out}, or outward rectifying K^+ channels [ORC]), have been identified in many plant cells, including guard cells (e.g., Blatt, 1992, 1997; Ilan et al., 1994; Roelfsema and Prins, 1998). Genes encoding K_H channels have been isolated from various plant sources: *kat1* (Anderson et al., 1992), *kat2* (Butt et al., 1997), *akt1* (Sentenac et al., 1992), *akt2* and *akt3* (Cao et al., 1995; Ketchum and Slayman, 1996) from *Arabidopsis thaliana*, *kst1* (Müller-Röber et al., 1995), *skt1* (Zimmermann et al., 1998), *skt2* and *skt3* (Ehrhardt et al., 1997) from potato *Solanum tuberosum*. KAT1 and KST1 represent guard cell K^+ uptake channels ($GCKC1_{in}$) (Cao et al., 1995; Nakamura et al., 1995; Dietrich et al., 1998), whereas AKT1 is present in the root to facilitate K^+ accumulation and hence plant growth (Lagarde et al., 1996; Hirsch et al., 1998).

Plant guard cells show robust electrical excitability, and both kinetic and steady-state electrical properties are modulated to serve their physiological needs, such as osmotic regulation, growth, and movements (Thiel et al., 1992; Gradmann et al., 1993; Schroeder et al., 1994). For example, in *Vicia faba* guard cells, the plant growth hormone auxin induces a train of action potentials (Blatt and Thiel, 1994). The guard-cell action potentials are characterized by intracellular pH-dependent oscillations of the membrane potential negative to the activation threshold of the K_H channel (Thiel et al., 1992; Roelfsema and Prins, 1998). The amplitude and frequency of the electrical oscillations, which differ notably in different plant species, at least in part, depend on the activation kinetics of K_H channels (Mummert and Gradmann, 1991; Thiel et al., 1992; Gradmann et al., 1993; Roelfsema and Prins, 1998). The $GCKC1_{in}$ (guard cell inward rectifiers) activation kinetics differ among various plant species (Fairley-Grenot and Assmann, 1993; Hedrich and Dietrich, 1996; Dietrich et al., 1998; Brüggemann et al., 1999b) and the diversity in the K^+ channel activation kinetics may contribute to the observed differences in the electrical excitability. This regulation of guard cell action potentials by $GCKC1_{in}$ is analogous to how kinetics of depolarization-activated K^+ channels in animal cells may regulate action potential generation and frequency (Hille, 1992).

Received for publication 10 June 1999 and in final form 3 December 1999.
Address reprint requests to Toshinori Hoshi, Department of Physiology and Biophysics, The University of Iowa, BSB 5–660, Iowa City, IA 52242. Tel.: 319-335-7845; Fax: 319-353-5541; E-mail: hoshi@hoshi.org.

0006-3495/00/03/1255/15 $2.00

Molecular and biophysical mechanisms of regulation of $GCKC1_{in}$, which, in turn, controls stomatal valves, have not been clearly elucidated. Studies using heterologously expressed KAT1-like channels show that both extracellular pH (pH_o) and intracellular pH (pH_i) may directly regulate kinetic and steady-state properties of the channel activation (Hedrich et al., 1995; Hoshi, 1995; Müller-Röber et al., 1995; Hoth et al., 1997; Hoth and Hedrich, 1999). The external pH sensor for KST1 appears to involve two histidine residues located in the P-segment and the extracellular S3–S4 linker segment (Hoth et al., 1997). In KAT1, the extracellular pH sensitivity is mediated by an amino acid residue in the P-segment (Hoth and Hedrich, 1999). Lower pH_i causes multiple changes in KAT1, including a shift in the steady-state macroscopic conductance–voltage ($G(V)$) curve to a more positive voltage (Hoshi, 1995). Qualitatively similar effects of pH_i have been reported for the K_H channels in native guard cells of broad bean *V. faba* (Grabov and Blatt, 1997).

The present study focuses on the molecular and biophysical mechanisms underlying the pH_i regulation of the activation kinetics of the cloned KAT1 channel. We show that the activation time course (T_A) of KAT1 is specifically controlled by histidine-118 in the putative cytoplasmic S2–S3 linker through an electrostatic interaction. We propose a simple linear kinetic scheme to account for the KAT1 activation where changes in one forward rate constant value could account for the effects of the mutations at position 118 in the voltage range where the channel open probability is saturated. Our results elucidate a molecular basis for the diversity in the activation kinetics of $GCKC1_{in}$ among different plant species, which allows them to respond to sudden changes in the environmental conditions.

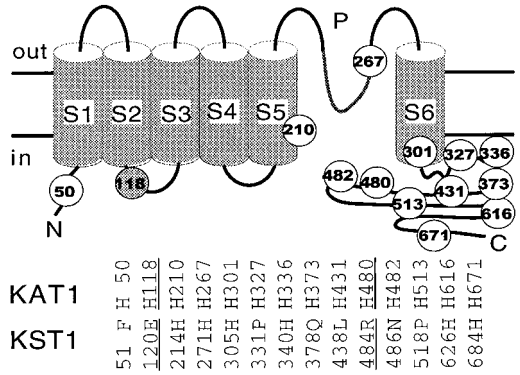

FIGURE 1 Diagram of the KAT1 channel α subunit. All 14 histidine residues are labeled, and histidine-118 in the putative S2–S3 linker is highlighted. The amino acid residues of the KST1 channel equivalent to the KAT1 histidine residues are aligned and shown below the diagram.

MATERIALS AND METHODS

Construction of mutant channels

Histidine residues in the KAT1 channel are illustrated in Fig. 1 and the histidine mutations prepared in this study are listed in Table 1. These mutants were constructed with the standard PCR-based mutagenesis protocol as described previously (López-Barneo et al., 1993) using the Pflm1 and Kpn1 sites in the KAT1 cDNA. The DNA segments amplified by PCR were sequenced (Applied Biosystems, The University of Iowa DNA Core Facility, Iowa City, IA). The KAT1 and KST1 cDNAs were linearized with Mlu1 and Sma1, respectively, and in-vitro transcribed using a T7 RNA polymerase kit (Ambion, Austin, TX).

Channel expression in oocytes

Xenopus laevis oocytes were surgically removed and treated with collagenase type 1A (Sigma, St. Louis, MO) as described (Hoshi et al., 1990) according to a protocol approved by the University of Iowa Animal Care and Use Committee. The amount of RNA injected was varied to give desired current levels. The oocytes were incubated at 18°C in ND96 solution (in mM): 96 NaCl, 2 KCl, 1 $MgCl_2$, 1.8 $CaCl_2$, 5 HEPES, 2.5 sodium pyruvate, pH 7.6.

The oocytes for patch clamp experiments were prepared by mechanically removing the vitelline membrane. Ionic currents through KAT1 and KST1 expressed in oocytes frequently run down or decrease in amplitude upon patch excision (Hoshi, 1995; Tang and Hoshi, 1999). To prevent or slow the rundown process and facilitate data acquisition and yet have an access to the intracellular compartment, we utilized the "bagel-like oocyte" approach to record the KAT1 and KST1 currents. In this protocol, we completely penetrated the oocyte with a pair of tweezers to form a large hole. The opening was typically greater than 50% of the oocyte diameter. The strong positive pressure from the patch pipette before the seal formation cleared away the egg yolk and enabled the seal formation. Cell-attached experiments were performed on these bagel-like oocytes and the bath solution in the chamber was then changed to manipulate the "internal" pH. The reversal potential experiments carried out using different K^+ concentrations indicated that it was possible to effectively change the internal ion concentrations (data not shown). Furthermore, the results obtained with these bagel-like oocytes were indistinguishable from those obtained using the true excised patch configuration.

TABLE 1 KAT1 histidine mutations tested in this study. The histidine residues, mutations and the electrophysiological functionality are listed

Histidine	Mutation	Function
H050	A	Yes
H118	A, N	Yes
	D, E	Yes
	R, K	Yes
H210	N	Yes
	A, C, P, V	No
H267	S	Yes
	G, V	No
H301	E	Yes
H327	Δ311–366	No
H336	Δ311–366	No
H373	Δ345–410	No
H431	Δ411–677	No
H480	Δ467–677	No
H482	Δ467–677	No
H513	Δ513–552	Yes
H616	Δ563–632	Yes
H671	Δ635–677	Yes

Plant material and protoplast isolation

The detailed protocols for the plant cell isolation were described elsewhere (Brüggemann et al., 1999b). Briefly, *A. thaliana* L. cv. Columbia (*Arabidopsis* Stock Center, Columbus, OH) were grown in a growth chamber with a light/dark cycle of 8/16 hr and a photon flux density of 300 μmol m^{-2} s^{-1} (HQ1-TS 250 W/D; Osram, München, Germany). The temperature was set at 22°C in the light and 16°C in the dark. The humidity ranged between 50 and 60%. Guard-cell protoplasts were enzymatically isolated from 5- to 7-week-old leaves of *A. thaliana* according to the method developed for *V. faba* (Hedrich et al., 1990).

Electrophysiology and data analysis

Macroscopic and single-channel currents were recorded with an Axopatch 200A amplifier (Axon, Foster City, CA) or an EPC-9 patch-clamp amplifier (HEKA, Lambrecht, Germany). Data acquisition was controlled by Pulse/PulseFit (HEKA) running on an Apple Power Macintosh computer equipped with an ITC-16 AD/DA interface (Instrutech, Port Washington, NY). The output of the clamp amplifier with the built-in filter at 5 kHz was low-pass filtered through a Bessel filter unit (Frequency Devices, Haverhill, MA) at 2 kHz and typically digitized at 2.5 kHz. Some data were filtered and digitized at different frequencies, however, the measured parameters were not noticeably affected. For the single-channel current analysis, the data were further filtered typically at 1 kHz using a Gaussian filter implemented in IgorPro (Wavemetrics, Lake Oswego, OR).

Oocyte macroscopic currents were recorded with borosilicate pipettes coated with dental wax, which had a typical resistance of 0.2~0.4 MΩ when filled with the solution described below. Macroscopic linear leak and capacitative currents were subtracted using a modified p/n protocol as implemented in Pulse. Single-channel KAT1 currents were recorded with borosilicate pipettes coated with Sylgard (Dow Corning, Midland, MI) and their resistance was typically 3~5 MΩ. For native guard-cell recordings, pipettes were prepared from Kimax-51 glass (Kimble, Vineland, NY) and coated with Sylgard. The command voltages were corrected off-line for liquid-junction potentials (Neher, 1992). Experiments were performed at room temperature (20–22°C).

The data were analyzed with custom routines implemented in IgorPro as described (Avdonin et al., 1997). Macroscopic and single-channel currents were simulated using BigChannel (T. Hoshi and D. Perkins).

Solutions

For oocyte recordings, the standard external (pipette) solution contained (in mM): 140 KCl, 2 $MgCl_2$, 10 HEPES, pH 7.2 adjusted with *N*-methylglucamine (NMG). The bath/internal solution typically contained (in mM): 140 KCl, 11 EGTA, 2 $MgCl_2$, 10 HEPES, pH 7.2 (NMG). Low and high internal pH solutions had the same composition as the standard solution, except that 10 mM MES replaced HEPES for pH 5.2 and pH 6.2 solutions and that 30 mM MOPS and 30 mM CAPS replaced HEPES for the pH 8.2 and pH 10.2 solutions, respectively. Some experiments were performed using AMPSO (30 mM) at pH 10.2, and the results were indistinguishable from those obtained using CAPS. With MES, the optimal pH buffer range is likely between pH 5 and 7. The lack of a better pH buffer for a lower range necessitated the use of MES (30 mM) for pH 4.4. The low-ionic strength internal solution contained (in mM): 224 sucrose, 28 KCl, 11 EGTA, 2 $MgCl_2$, 10 HEPES, pH 7.2 (NMG). For guard-cell recordings, the bath solution contained (in mM): 30 potassium gluconate, 1 $CaCl_2$, pH 5.6 (10 MES/Tris). The pipette solutions contained (in mM): 150 potassium gluconate, 10 EGTA, 2 $MgCl_2$, 1 ATP (Mg^{2+} salt), pH 5.5–8 (HEPES, MES, MOPS/Tris where appropriate). The osmolarity was adjusted to 550 mosmol/kg with D-sorbitol.

RESULTS

Internal pH regulates the activation time course of KAT1 expressed in *Xenopus* oocytes and $GCKC1_{in}$ in native *Arabidopsis* guard cells

The activation time course or T_A of the KAT1 channel expressed in *Xenopus* oocytes is regulated by pH_i. Figure 2 *A* shows representative normalized current traces recorded at the pH_i values indicated. All the currents were elicited by voltage pulses (V_P) to −180 mV from a holding potential (V_H) of 0 mV. T_A was markedly faster at low pH_i than at high pH_i. Because T_A of the KAT1 channel is best described by a sum of more than two exponentials (see later in this

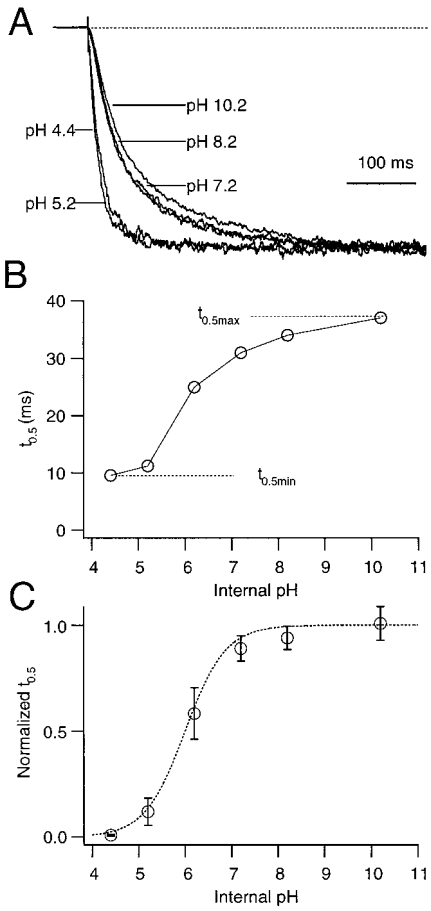

FIGURE 2 pH_i dependence of KAT1 activation time course. (*A*) Scaled representative KAT1 currents from membrane patches recorded at different pH_i values as indicated. The currents were obtained from a bagel-like oocyte bathed in internal solutions with different pH at a pulse voltage (V_P) of −180 mV. Pipette solution contained 140 mM KCl, pH 7.2. (*B*) pH_i dependence of the half-activation time ($t_{0.5}$). The $t_{0.5}$ values are plotted against different pH_i tested. (*C*) Henderson–Hasselbalch plot of the normalized $t_{0.5}$–pH_i relations. The $t_{0.5}$ values at different pH_i are transformed to the normalized $t_{0.5}$ values, which are calculated as $(t_{0.5} - t_{0.5min})/(t_{0.5max} - t_{0.5min})$. The mean $t_{0.5}$ at $pH_i = 10.2$ is taken as $t_{0.5max}$ ($n = 5$) and the mean $t_{0.5}$ at $pH_i = 4.4$ is taken as $t_{0.5min}$ ($n = 3$). The *dashed* curve represents the titration curve of a single histidine residue ($pK = 6.0$) in solution.

section; also see Zei and Aldrich, 1998), we used the time required for the current to reach 50% of the maximum value ($t_{0.5}$) as an operational measure to describe the pH_i dependence of T_A (Hedrich et al., 1995). As shown in Fig. 2 *B*, the activation kinetics of the KAT1 channel was regulated by pH_i most notably in the pH range of 5.2 to 8.2. The $t_{0.5}$ values were more than three times greater at $pH_i = 8.2$ than at $pH_i = 5.2$ and reached the maximum at $pH_i = 9$ and the minimum at $pH_i = 5.2$. We normalized the pH_i dependence of $t_{0.5}$ using the maximal and minimal values observed at the extreme pH_i values. The results obtained from different experiments were fitted with the standard Henderson–Hasselbalch pH titration equation (Fig. 2 *C*). The normalized pH_i dependence of $t_{0.5}$ suggests that the overall T_A had a pK value of 6.0, which is close to the value often reported for a free histidine in solution (Edsall and Wyman, 1958). These results suggest that an intracellular histidine residue might be responsible for the observed pH_i regulation of the KAT1 T_A, although other mechanisms exist to account for physiological processes having pK values near 6–7 (Coulter et al., 1995; Fakler et al., 1996; Hoth et al., 1997).

Representative single-channel openings of the KAT1 channel obtained at two different pH_i values are shown in Fig. 3 *A*. Consistent with the macroscopic results, low pH_i accelerated the channel opening. The first latency distributions of the single-channel KAT1 openings obtained at two different pH_i (6.2 and 7.2) are compared in Fig. 3 *B*. The median first latency at $pH_i = 6.2$ (31 ± 10 ms, $n = 3$, −120 mV) was markedly faster than that at $pH_i = 7.2$ (327 ± 50 ms, $n = 3$, −120 mV). However, after the channel opened, the open and closed time distributions were very similar at $pH_i = 6$ (mean open duration: 16.1 ± 2.2 ms, mean closed duration: 3.2 ± 0.6 ms, $n = 4$, −160 mV) and $pH_i = 7.2$ (mean open duration: 15.2 ± 1.5 ms, mean closed duration: 3.1 ± 0.3 ms, $n = 5$, −160 mV). The results suggest that pH_i does not affect the gating transitions after the channel opens.

KAT1 is mainly expressed in plant guard cells (Cao et al., 1995; Nakamura et al., 1995), and it is likely to represent the dominant component of *A. thaliana* $GCKC1_{in}$. At least qualitatively, the native $GCKC1_{in}$ of *A. thaliana* is similar to the heterologously expressed KAT1 in many electrophysiological properties, although some differences have been observed (Dietrich et al., 1998; Brüggemann et al., 1999b). We investigated whether the activation kinetics of $GCKC1_{in}$ of *A. thaliana* is regulated by pH_i in a similar manner. Fig. 4 *A* shows representative current records from a native

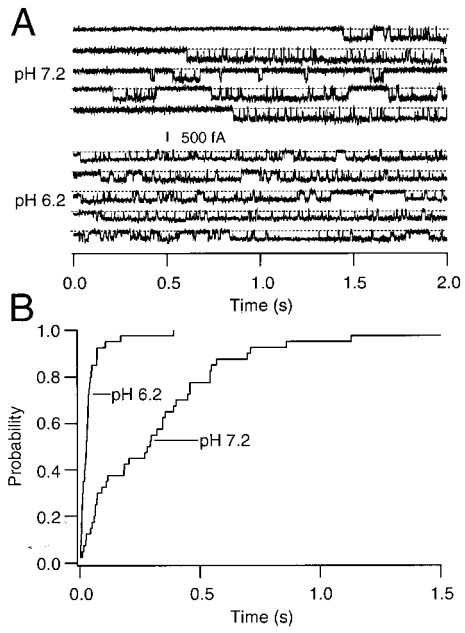

FIGURE 3 Comparison of the first latency distributions for KAT1 at different pH_i. (*A*) Representative single-channel KAT1 currents recorded at $pH_i = 7.2$ (*upper panel*) and 6.2 (*lower panel*). The currents were elicited by V_P to −120 mV from a holding voltage of 0 mV every 12 s. Only the initial 2-s segments are shown. Downward deflections indicate the openings. Leak and capacitative currents were subtracted. To slow rundown, ATP (3 mM) was added in the bath solution. (*B*) First-latency distributions for the data shown in (*A*). Each distribution was constructed from 40 sweeps.

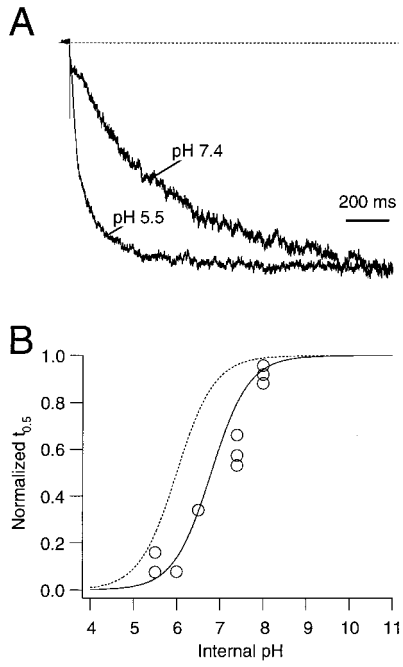

FIGURE 4 pH_i dependence of $GCKC1_{in}$ activation time course. (*A*) Representative whole-cell $GCKC1_{in}$ current traces recorded at −196 mV from two guard cell protoplasts at pH 7.4 and 5.5, respectively. Consistent with a previous report (Brüggemann et al., 1999b), the activation kinetics of the heterologously expressed KAT1 is faster than that of native $GCKC1_{in}$. (For discussion, see Brüggemann et al., 1999b). In this case, $t_{0.5}$ values were determined from 1500 ms sweeps, which still underestimate the $t_{0.5}$ values especially at more alkali pH. However, when normalized, the $t_{0.5}$–pH relation of $GCKC1_{in}$ (see *B*) is similar to that of KAT1 as shown in Fig. 2 *C*. (*B*) Henderson–Hasselbalch plot of the normalized $t_{0.5}$–pH_i relations of $GCKC1_{in}$. The normalization was done in the same way as in Fig. 2 *C*. The solid curve represents the titration curve of an amino acid with a pK of 6.7 and the *dashed* curve reflects that of a histidine residue (KAT1) (pK = 6.0) in solution.

guard cell protoplast at two pH_i values. As found with KAT1 expressed in oocytes, low pH_i accelerated T_A $GCKC1_{in}$. The normalized $t_{0.5}$–pH curves obtained from several measurements (Fig. 4 *B*) suggest that $GCKC1_{in}$ and KAT1 are regulated by pH_i in a similar fashion. These results further indicate that regulation of KAT1 by pH_i is a physiologically relevant phenomenon. It should be noted that, although they are similarly regulated by pH_i, T_A of KAT1 heterologously expressed in oocytes is faster than that of $GCKC1_{in}$ (cf. Fig. 1 and Fig. 4; also see Brüggemann et al., 1999b). It is not clear what accounts for this difference. Differential phosphorylation status (Tang and Hoshi, 1999) or the auxiliary subunits (Tang et al., 1996) could potentially contribute to the slower kinetics of $GCKC1_{in}$.

Positively charged residues at position 118 accelerate the activation time course but render the channel less pH-sensitive in the physiological pH range

The pH_i dependence of the KAT1 macroscopic activation kinetics (Fig. 2 *C*) suggests that histidine may be involved. As illustrated in Fig. 1, most histidine residues are found in the cytoplasmic carboxyl segment of the KAT1 channel protein. However, H513, H616, and H671 are not likely to be involved because these residues can be deleted without any marked change in the activation kinetics (see KAT1Δ513–552, KAT1Δ563–632, and KAT1Δ635–677 in Table 1; also see Marten and Hoshi, 1997, 1998). The deletion mutants covering H327, H336, H373, H431, H480, and H482 (KAT1Δ311–366, KAT1Δ345–410, KAT1Δ411–677, and KAT1Δ467–677) did not result in functional expression and their roles remain unknown (Table 1; also see Marten and Hoshi, 1997, 1998). H50, H210, H267, and H301 could be replaced without affecting the activation kinetics either (data not shown). Thus, we hypothesized that histidine-118 located in the putative cytoplasmic S2–S3 linker segment might underlie the pH_i dependence of the KAT1 T_A. According to this hypothesis, substitution of H118 with a positively charged amino acid should accelerate T_A, whereas a negatively charged amino acid should slow it. We replaced histidine-118 by a variety of charged amino acids as listed in Table 1 and all these mutants were electrophysiologically functional. Normalized representative currents recorded from the wild type KAT1 (this channel will be referred to as H118H), H118K, H118R, H118D, and H118E channels at $pH_i = 7.2$ in response to voltage pulses to −180 mV are shown in Fig. 5 *A*. The H118K and H118R channels with a positively charged amino acid at position 118 activated markedly faster than the H118H channel at $pH_i = 7.2$. However, T_A of H118K and H118R, with two very different side chain structures (Richardson and Richardson, 1989) but the same positive charge, were virtually indistinguishable. The negatively charged amino acid mutants, H118D and H118E, were noticeably slower in their activation kinetics than the H118H channel but again very similar to each other. These observations are consistent with the interpretation that the side chain charge status at position 118 is a prominent determinant of KAT1 T_A.

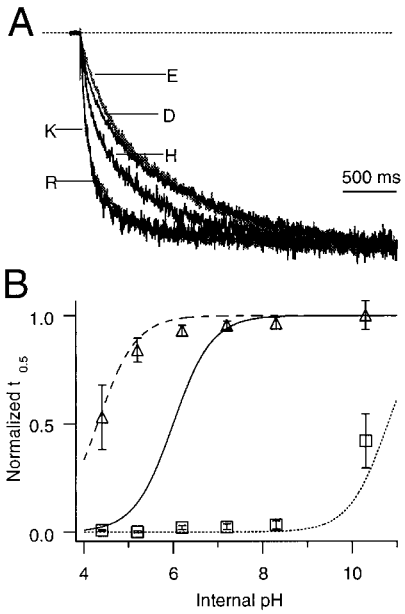

FIGURE 5 Effects of charged amino acids at position 118 on activation time course. (*A*) Representative T_A for the channels with different amino acid residues at position 118 as indicated. $VP = -180$ mV, $pH_i = 7.2$. (*B*) Henderson–Hasselbalch plot of the normalized $t_{0.5}$–pH_i relations for the H118E and H118K mutants. Each point represents the mean of 3–5 measurements. For H118K and H118E, the $t_{0.5max}$ and $t_{0.5min}$ values of wild type KAT1 were used because it was difficult to determine the extreme values for these mutant channels. The *dashed* curve and *dotted* curve are the titration curves of a single glutamate residue (pK = 4.3) or a lysine residue (pK = 10.8) in solution, respectively. Histidine titration curve (*solid* curve) is also plotted for comparison.

The pH_i dependence of T_A in the H118 mutants is shown in Fig. 5 *B* using $t_{0.5}$ as the operational measure. Within the pH_i range of 5.2 to 8.2, where H118H is very pH_i sensitive (see Fig. 2), neither H118E nor H118K showed any marked pH_i dependence. Activation time course of H118E remained slow and mostly independent of pH_i and that of H118K remained fast and also independent of pH_i in this pH range (Fig. 5 *B*). These results suggest that the pH_i dependence of H118H in the physiological pH range of 5.2 to 8.2 is mediated by the charge status of H118 in the S2–S3 linker segment. At the extreme pH_i values, however, both H118E and H118K exhibited some pH_i dependence. For example, H118E T_A was noticeably and consistently faster at $pH_i = 4.2$ than that at $pH_i = 5.2$, and H118K T_A was slower at $pH_i = 10.2$ than at 8.2 (Fig. 5 *B*). The pH_i dependence of T_A at the extreme pH_i values may reflect pKs of the side chains in E and K, which are about 4.3 and 10.8 in solution, respectively (Edsall and Wyman, 1958). Because $t_{0.5min}$ for H118E and $t_{0.5max}$ for H118K could not be obtained, the pH_i dependence data were not confidently fitted with the Hend-

erson–Hasselbalch formulation. However, using pK values of 4.3 and 10.8, which are often described for the side chains of E and K (Edsall and Wyman, 1958), the small pH_i dependence of H118E and H118K could be approximated (Fig. 5 *B*). It is also possible that structural determinants other than the amino acid at position 118 are involved in regulating the small pH_i sensitivities of the H118E and H118K mutant channels.

Position 118 may account for the difference in activation kinetics of the KAT1 and KST1 channels

KST1 is another member of the KAT family cloned from potato *S. tuberosum* (Müller-Röber et al., 1995). In native guard cells, $GCKCl_{in}$ from potato (KST1 being the dominant component) activates more slowly than that from *A. thaliana* (Hedrich and Dietrich, 1996; Dietrich et al., 1998). A sequence analysis reveals that the overall amino acid identity between KAT1 and KST1 is about 60% and many primary structural domains that are believed to be involved in the channel gating, such as the S4 segment, are identical (Müller-Röber et al., 1995; Nakamura et al., 1995). Nevertheless, at the H118-equivalent position, a glutamate residue (E) is found in KST1. The results that T_A of H118E is slower and less pH_i-dependent than that of H118H predict that T_A of KST1 with E at the H118-equivalent position should be slower than that of H118H and similar to that of H118E. Normalized representative currents through H118H, H118E, and KST1 measured at $pH_i = 7.2$ are compared in Fig. 6 *A*. Consistent with the prediction, T_A of KST1 was slower than that of H118H and indistinguishable from that of H118E (Fig. 6 *A*; also see Fig. 5 of Hedrich and Dietrich, 1996). Furthermore, the activation time course of KST1 was much less dependent on pH_i than that of H118H but very similar to that of H118E. Within the physiological pH_i range (6.2 and 8.2), T_A of KST1 was essentially independent of pH_i (Fig. 6 *B*, $n = 2–4$). At extreme lower pH_i, as found with H118E, KST1 T_A accelerated (Fig. 6 *B*). We also recorded the $GCKCl_{in}$ currents from native guard cells of potato and *A. thaliana* and confirmed the kinetic difference between the two species (data not shown but see Hedrich and Dietrich, 1996; Dietrich et al., 1998). Therefore, it is concluded that the KAT1 H118-equivalent position in KST1 also plays an important role in determining KST1 T_A and pH_i sensitivity.

Noncharged amino acid residues at position 118 render the channel less pH_i sensitive

The above results suggest that a positively charged amino acid accelerates whereas a negatively charged amino acid at position 118 slows KAT1 T_A, and that protonation/deprotonation of histidine-118 plays a major role in the KAT1

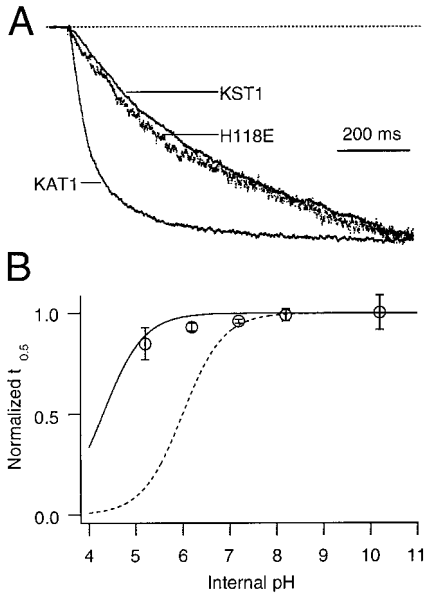

FIGURE 6 Activation time course of H118H, H118E, and KST1. (*A*) Scaled representative currents for H118H, H118E, and KST1 elicited at −180 mV, $pH_i = 7.2$. (*B*) Henderson–Hasselbalch plot of the normalized $t_{0.5}$–pH_i relation for KST1. Each point represents the mean of 2–4 measurements. Histidine titration curve (*dotted* curve) is plotted for comparison.

pH_i sensitivity. This model predicts that substitution of histidine-118 with a noncharged amino acid residue should render KAT1 T_A less sensitive to pH_i without markedly affecting T_A around $pH_i = 7$ because histidine may be neutral at this pH. Normalized representative currents through H118H, H118N, and H118A recorded at −180 mV and $pH_i = 7.2$ are compared in Fig. 7 *A*. As predicted, T_A was not noticeably different among these channels (Fig. 7 *A*, *right*, $n = 5$), suggesting that the side chain charge status is indeed important in determining KAT1 T_A. The H118A and H118N T_A was still dependent on pH_i but to a lesser extent. Increasing pH_i from 5.2 to 8.2 typically slowed H118H $t_{0.5}$ 3–4-fold. However, the same pH_i change induced only about a 2-fold change in H118N $t_{0.5}$ (Fig. 7 *B*). More noticeably, the $t_{0.5}$–pH_i relation of H118N was much less steeper than that of H118H and the normalized pH_i dependence could no longer be well described by a simple Henderson–Hasselbalch formulation (Fig. 7 *B*, *right*). These results again indicate that the charge status at position 118 contributes to the pH_i sensitivity of the wildtype KAT1 channel. The results suggest that additional mechanisms may control the pH_i dependence of T_A because H118A and H118N exhibited smaller and shallower but still noticeable pH_i dependence.

Deactivation kinetics is not affected by mutations at position 118

The effect of the H118 mutations was specific to T_A and the mutations did not affect the deactivation time course (T_{DA}).

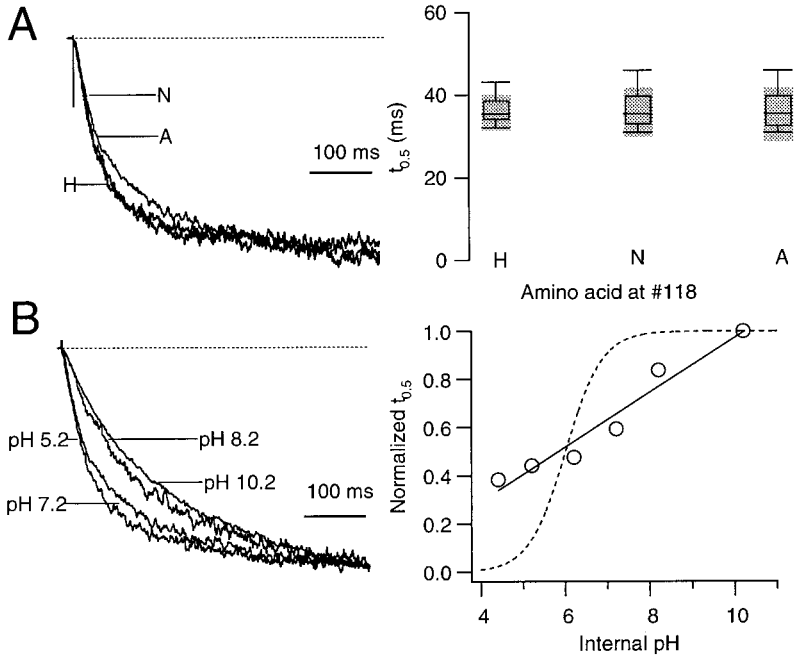

FIGURE 7 Activation time course of H118A and H118N. (*A*) Comparison of T_A of H118H, H118A, and H118N. Scaled representative current traces for H118H, H118A, and H118N recorded at $pH_i = 7.2$. *V*P = −180 mV (*left*). Box plots of $t_{0.5}$ for H118H, H118A, and H118N (*right*). (*B*) Effects of pH_i on the H118N mutant. Representative current traces elicited at −180 mV and different pH_i (*left*). Normalized $t_{0.5}$–pH_i relation for the H118N channel (*right*). The $t_{0.5}$ values were normalized to the mean value obtained at $pH_i = 10.2$. The *solid* line is a linear fit to the data without any theoretical significance. For comparison, the histidine titration curve is plotted.

Normalized representative tail currents of H118K, H118D, and H118N recorded at +60 mV are compared in Fig. 8 *A*, and they were indistinguishable. The voltage dependence of the tail currents recorded from the H118H and other H118 mutant channels at $pH_i = 7.2$ is shown in Fig. 8 *B*. Because the closing transitions near the open state play dominant roles in determining T_{DA}, the results suggest that the H118 mutations do not affect these closing transitions of the KAT1 channel.

Steady-state activation properties are only slightly affected by mutations at position 118

Although the H118 mutations have profound effects on KAT1 T_A (see Fig. 3), they only slightly altered the normalized macroscopic $G(V)$ provided that the hyperpolarization epoch durations were sufficiently long. Representative macroscopic currents from H118H, H118R, and H118D elicited at various voltages and their macroscopic $G(V)$ curves are shown in Fig. 9. As demonstrated in Figs. 5 and 8 *C*, T_A of H118D is markedly slower. However, the steady-state macroscopic $G(V)$ curves of the H118 mutants obtained using hyperpolarization pulses >5 s in duration closely resembled each other. The voltage dependence of both the wild type and mutant channels was only slightly altered, and the macroscopic $G(V)$ curves could be well approximated by the fourth power of a Boltzmann function with the half-activation voltage ($V_{1/2}$) of −74 mV with an equivalent charge of 1.5 e_0 ($n = 13$). The small shift in $G(V)$ found for the H118D mutant may be caused by hyperpolarizing pulses that were not sufficiently long enough for the channel activation to reach the steady state.

Mutations at position 118 alter the first latency without affecting the transitions after opening

We investigated the changes in the KAT1 channel gating induced by the H118 mutations at the single-channel level. Representative single-channel openings of H118H and H118D are shown in Fig. 10 *A*. The most obvious difference between H118H and H118 mutants was their first latency property. This is illustrated by the first latency distributions of H118H and H118D in Fig. 10 *B*. Consistent with the macroscopic current results presented earlier, the first latency distribution of H118D at −160 mV was markedly slower than that of H118H. The average median first latencies for H118H and H118D were 96 ± 17 ms ($n = 4$) and 410 ± 47 ms ($n = 4$), respectively. Because the open probability (p_o) is nearly saturated at −160 mV (Fig. 9 *A*), the forward opening rate constants are expected to be much greater than the backward closing rate constants (Zei and Aldrich, 1998). Thus, the difference in the first latency suggests that the H118 mutations specifically alter the forward opening transitions of the KAT1 channel. In contrast, after the channels opened, the gating properties of the H118 mutants were indistinguishable. The steady-state p_o values for H118H and H118 mutants were calculated directly from the single-channel currents recorded in response to various voltage steps, excluding the first latency closed events. Figure 10 *C* shows that the p_o values for different H118 mutants were very similar at all the voltages examined, suggesting that the gating transitions after the channels open are similar. Analysis of the open and closed durations also supports the idea that only the transitions leading up to the first opening are affected by the H118 mutations. The open

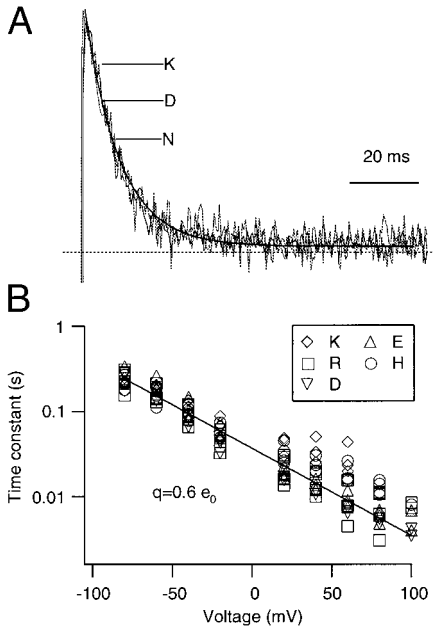

FIGURE 8 Deactivation of the H118H and H118 mutant. (*A*) Representative tail currents from H118N, H118D, and H118K. The currents were recorded at +60 mV following prepulses to −180 mV to activate most of the channels, $pH_i = 7.2$. At this voltage, T_{DA} can be fitted with a single exponential as indicated by the smooth curve. (*B*) Comparison of the deactivation time constant (τ_{DA})-voltage curves ($\tau_{DA}(V)$) for the H118H and selected H118 mutant channels on semilogarithmic plot. The $\tau_{DA}(V)$ relations for the H118H and H118 mutants at this pH_i could be well described by a single-exponential function, with an equivalent charge of 0.6 e_0.

and closed duration histograms were constructed from representative single-channel currents recorded at −160 mV from H118H and H118D (Fig. 11). These dwell-time distributions were nearly indistinguishable. The mean open durations were 15.2 ± 1.5 ms ($n = 5$) and 15.3 ± 1.6 ms ($n = 5$), and the mean closed durations were 3.1 ± 0.3 ($n = 5$) ms and 3.1 ± 0.2 ms ($n = 5$) for H118H and H118D, respectively. Similar results were observed for other H118 mutants (data not shown).

Single-channel current amplitudes are not affected by the H118 mutations

Although the first latencies are affected by the charged H118 mutations, the single-channel amplitudes of the H118 mutants (H118D, H118E, H118K, and H118R) were very similar to that of the wild type KAT1 channel. This finding can be seen in the representative single-channel currents recorded from H118H and H118D shown in Fig. 10 *A*. No significant difference in the current amplitude is observed among these different channels ($n = 5$), indicating that the ion-conduction properties are not affected by the H118 mutations.

Changes in bulk ionic strength do not alter the activation kinetics

The H118 mutation results show that a positively charged amino acid at position 118, whether K, R, or protonated H, accelerates T_A to about the same extent, and that a negatively charged amino acid residue slows down the process. A noncharged amino acid, such as A or N, does not affect T_A at $pH_i = 7.2$. These results suggest that the residue 118 may electrostatically interact with its effector site to regulate the channel opening transition. We examined this hypothesis by manipulating the ionic strength of the internal solution. Bulk electrostatic interactions are expected to be strengthened by lowering the ionic strength and weakened by increasing the ionic strength. The macroscopic currents of H118H and H118E were recorded in the solutions of different ionic strength. However, T_A of both H118H and H118E at $pH_i = 6.2$ where H118 is expected to be proton-

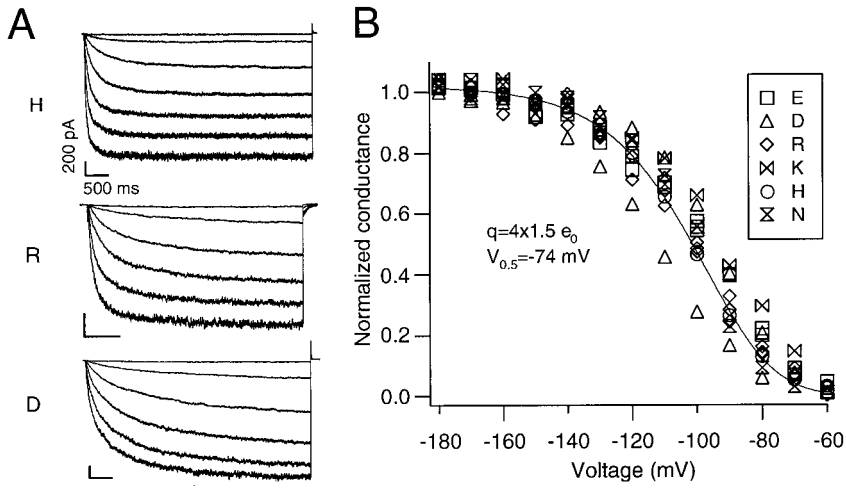

FIGURE 9 Steady-state macroscopic activation of the H118H and H118 mutant. (*A*) Macroscopic current families from H118H, H118R, and H118D. The currents were recorded in response to 5-s V_P from −60 to −180 mV in 10-mV increments and then switched to +70 mV (H118H and H118D). For H118R, the currents were recorded in response to 4-s V_P from −60 to −180 mV in 10-mV increments and then to −50 mV. The time 0 current amplitude of each tail current was obtained by a single-exponential fit. (*B*) Normalized $G(V)$ curves for the H118H and H118 mutant channels. These data could be reasonably approximated by a fourth power of Boltzmann function with $V_{0.5} = -74$ mV and $q = 1.5$ e_0 ($n = 13$).

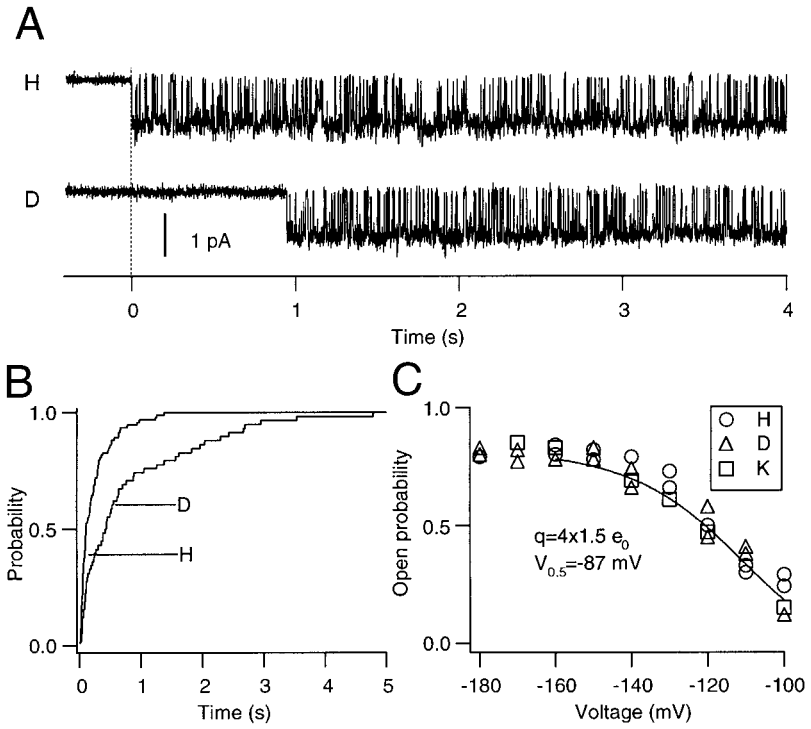

FIGURE 10 Effects of the amino acid at position 118 on the single-channel currents. (*A*) Representative single-channel currents for H118H and H118D that were elicited by a 60-s hyperpolarizing pulse to −160 mV from 0 mV, $pH_i = 7.2$. Downward deflections indicate the opening transitions. Note the prolonged first latency of the H118D channel. (*B*) Comparison of the first latency distributions for H118H and H118D. The first-latency distribution shows the probability that the channel has opened for the first time by the time indicated. To construct the first latency distributions for H118H and H118D, 56 and 78 hyperpolarization epochs were used respectively. (*C*) Comparison of the $p_o(V)$ relations for H118H, H118D, and H118K. The data could be approximated by a fourth power Boltzmann function with $V_{0.5} = -87$ mV and $q = 1.5\ e_0$. Note the similarity of these single-channel results and the macroscopic data as shown in Fig. 9 *B*.

ated, was not markedly affected by the changes in the internal solution ionic strength (data not shown). Thus, the electrostatic interactions in the bulk internal medium are not likely to be involved in the KAT1 T_A regulation by pH_i. Manipulations of the bulk ionic strength, however, may not affect local electrostatic interactions in confined areas.

To determine whether the total global charge near the amino acid residue 118 is important in determining the activation kinetics, we constructed the H118Rx3 and H118Dx3 mutants, where histidine-118 was replaced with three arginine or aspartate residues, respectively. Unfortunately, these mutants did not functionally express.

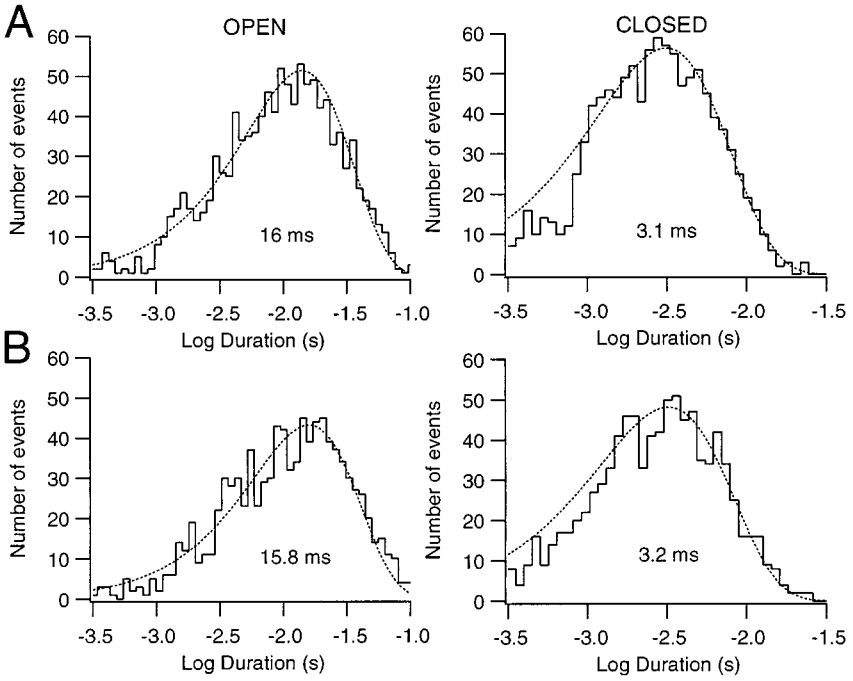

FIGURE 11 Comparison of the open and closed time durations for H118H and H118D. (*A*) Open and closed durations of the currents recorded from a single H118H channel as shown in Fig. 10 *A*. Both histograms could be well fitted by a single-exponential function. (*B*) Open and closed durations of the currents recorded from a single H118D channel. The time constants estimated were similar to those of the wild type KAT1 channel.

Changes in one forward rate constant simulate the effects of mutations at position 118

To account for the observed effects of the H118 mutations on KAT1 activation, we propose a simple linear kinetic scheme for the KAT1 activation time course, which is constrained by our experimental results as discussed below. The main scope of this modeling process is to describe T_A of the KAT1 channel and how the H118 mutations may modify the model parameters.

First, our single-channel current analysis revealed that the open durations of KAT1 could be well fitted with a single exponential (Fig. 11 *A*; also see Zei and Aldrich, 1998; Tang and Hoshi, 1999), suggesting that KAT1 has only one open state.

Second, KAT1 T_A follows a sigmoidal time course as predicted by linear multiclosed-state models (Hoshi, 1995; Zei and Aldrich, 1998). This sigmoidal nature is illustrated in Fig. 12 *A* using the normal and semilogarithmic time axes. The simplest model to account for the sigmoidal delay is given in Scheme 1. At −180 mV, the open probability is saturated, and the backward closing rate constant values are likely to be negligible (Zei and Aldrich, 1998). Thus, Scheme 1 has two free parameters, k_{01} and k_{12}.

$$C0 \underset{k_{10}}{\overset{k_{01}}{\rightleftharpoons}} C1 \underset{k_{21}}{\overset{k_{12}}{\rightleftharpoons}} O2$$

SCHEME 1

Third, as shown in Fig. 12, a prominent slow phase in KAT1 T_A was observed (see the current between $t = 0.1$ and 2 s in Fig. 12 *A*, *right panel*). The initial sigmoidal activation characteristic was well described by Scheme 1 involving two sequential closed states (Fig. 12 *B*). However, the whole T_A of KAT1 could not be well fit by a sum of two exponentials because of the slow phase in T_A (Fig. 12 *A*).

This slow component in T_A is not likely to be caused by the endogenous channels in oocytes because it was observed regardless of the number of channels expressed (data not shown). The presence of this slow phase suggests that, in addition to the two closed states in Scheme 1, KAT1 may transverse additional closed states before opening. A similar observation regarding the slow component was also made by Zei and Aldrich (1998).

To account for the slow activation component, the following model may be considered (Scheme 2), in which one additional closed state (C3) is included.

$$\begin{array}{ccccc} C0 & \underset{k_{10}}{\overset{k_{01}}{\rightleftharpoons}} & C1 & \underset{k_{21}}{\overset{k_{12}}{\rightleftharpoons}} & O2 \\ k_{30}\uparrow\downarrow k_{03} & & & & \\ C3 & & & & \end{array}$$

SCHEME 2

Scheme 2 postulates that the initial sigmoidal characteristic of the current is primarily described by the two opening rate constants k_{01} (fast) and k_{12} (slow) and that the slow component is described by the delayed activation of the channels that visited C3. The measured macroscopic KAT1 current and the current predicted by Scheme 2 with the rate constants indicated are compared in Fig. 13. We attempted to fit the current time course by manipulating the values of

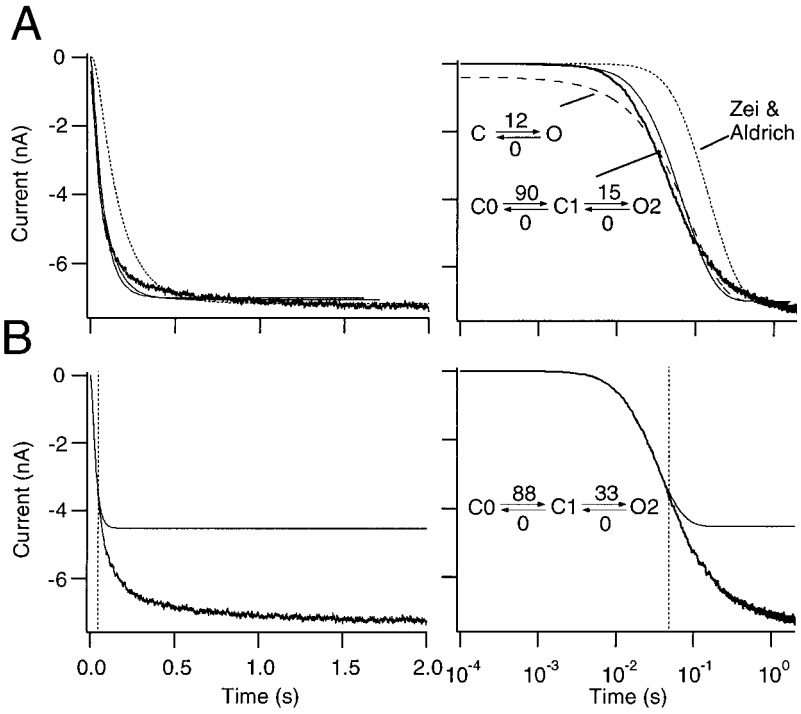

FIGURE 12 Comparison of the measured KAT1 current and that predicted by the two-state and three-state models. (*A*) Current time courses predicted by a simple two state (closed-open) model, the three-state (closed-closed-open) model and the Zei and Aldrich model (1998). The model parameters were adjusted to fit the entire current time course. *Left*, linear time scale; *right*, semilogarithmic time scale. At time $t = 0$, all the channels were assumed to be in C or C0. (*B*) The sigmoidal activation kinetics predicted by Scheme 1. The current segment between time $t = 0$ and the half-maximum amplitude time as indicated by the dashed vertical line was fitted with Scheme 1. The rate constant values used are shown.

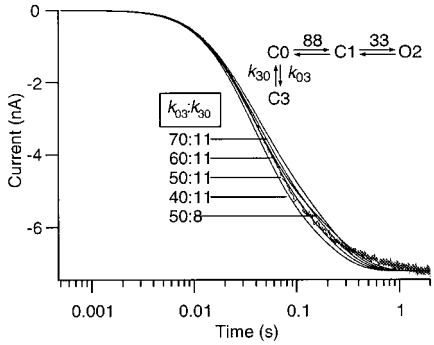

FIGURE 13 Scheme 2 predictions. Activation time course of KAT1 as predicted by Scheme 2. Several predictions of Scheme 2 using different parameter values (*thin smooth lines*) are also shown superimposed on the measured wild type KAT1 T_A. The currents were simulated using the rate constant values as shown. At time $t = 0$, all the channels were assumed to be in C0. None of the predicted currents adequately match the slow activation phase.

k_{03} and k_{30}. The best fit obtained using Scheme 2 is shown in Fig. 13, along with those predicted using other values for k_{03} and k_{30}. The fit was not satisfactory regardless of the values of k_{03} and k_{30} (see the current between 0.1 and 1 s in Fig. 13).

To adequately simulate the slow activation component of the macroscopic KAT1 current, we found that one additional closed state was necessary, as arranged in Scheme 3:

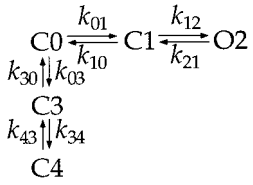

SCHEME 3

To describe the single-channel KAT1 behavior such as the fast flickers (Zei and Aldrich, 1998; Tang and Hoshi, 1999), a short-lived closed state (C5) was added to Scheme 3, generating the following model:

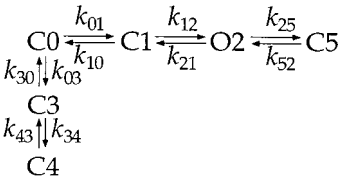

SCHEME 4

Scheme 4 accounts for most of the observations reported in this study. The currents simulated by the model at two different voltages are shown in Fig. 14 *A*. The values of k_{01} and k_{12} were obtained by fitting Scheme 1 to the current segment between the beginning and 50% of the maximal amplitude at different voltages between −200 and −130 mV (Fig. 12 *B*). The value of k_{12} was also determined from the double-pulse reactivation experiments, and the results using these two protocols were similar (data not shown). The voltage dependence of k_{01} and k_{12} was assumed to be described by $k_{01}(V) = k_{01(0)} * \exp(z_{01} * V/kT)$ and $k_{12}(V) = k_{12(0)} * \exp(z_{12} * V/kT)$ where $k_{01(0)}$ and $k_{12(0)}$ represent the values of k_{01} and k_{12} at 0 mV, z_{01} and z_{12} are their equivalent charges, and $kT = 25$ mV. The estimated values of $k_{01(0)}$ (z_{01}) and $k_{12(0)}$ (z_{12}) from a representative experiment were 0.57 s^{-1} (−0.7 e_0) and 8 s^{-1} (−0.2 e_0), respectively (Fig. 14 *A*). Although the values of the rate constants at 0 mV, $k_{01(0)}$ and $k_{12(0)}$, required small adjustments (typically, 0.49–0.63 s^{-1} for $k_{01(0)}$ and 6.5–8 s^{-1} for $k_{12(0)}$, $n = 5$), their voltage dependence, z_{01} (0.69 ± 0.03, $n = 5$) and z_{12} (0.19 ± 0.02, $n = 5$) showed little variation in the different data sets analyzed. The values of k_{25} and k_{52} were obtained from the single-channel mean open and closed durations as described elsewhere (Tang and Hoshi, 1999). The higher value of k_{52} relative to the overall T_A necessitates the placement of C5 after the opening state. The values of k_{03}, k_{30}, k_{34}, and k_{43} were manually adjusted so that the simulated currents well matched the observed data as judged by eye (refer to the Fig. 14 legend for the parameter value ranges examined). We found that it was possible to simulate T_A without assuming any voltage dependence in k_{30}, k_{03}, k_{43}, or k_{34}. The model satisfactorily describes KAT1 T_A in the range of −130 to −200 mV, where p_o is saturated, and k_{10} and k_{21} are assumed to be negligible.

Using Scheme 4 with the parameters optimized to fit the wild type KAT1 activation, it is possible to account for the effects of the H118 mutations by adjusting the value of a single rate constant, k_{01}. We found that the effects of the H118 mutations could be simulated by adjusting $k_{01(0)}$ without altering its voltage dependence (z_{01}). Specifically, to describe the effects of H118D mutation in the voltage range of −130 to −200 mV, $k_{01(0)}$ was decreased by ~65%, from 0.57 to 0.2 s^{-1} ($n = 3$), without changing its equivalent charge. The measured and simulated macroscopic currents for the wild type and H118D channels at −180 and −150 mV are compared in Fig. 14 *A*. The similarity between the measured and simulated data indicates that the model adequately approximates the effects of the H118 mutations described in this study.

Manipulations of the rate constants among C4, C3, and C0 were not able to simulate the H118D's effect, because changes in the values of k_{03}, k_{30}, k_{34}, and k_{43} compromised the sigmoidal characteristic of the activation kinetics (data not shown). Manipulations in the two rate constants involved in the single-channel burst behavior, k_{25} and k_{52}, did not simulate the effect of the H118D mutations, consistent with the observation that the burst behavior was not altered in the H118D mutations (Figs. 10 *A* and 11). Changes in the k_{12} value did not produce satisfactory results to simulate the H118 data. Representative KAT1 wild type and H118D single-channel currents at −180 mV simulated using Scheme 4 are shown in Fig. 14 *B*. The simulated data well

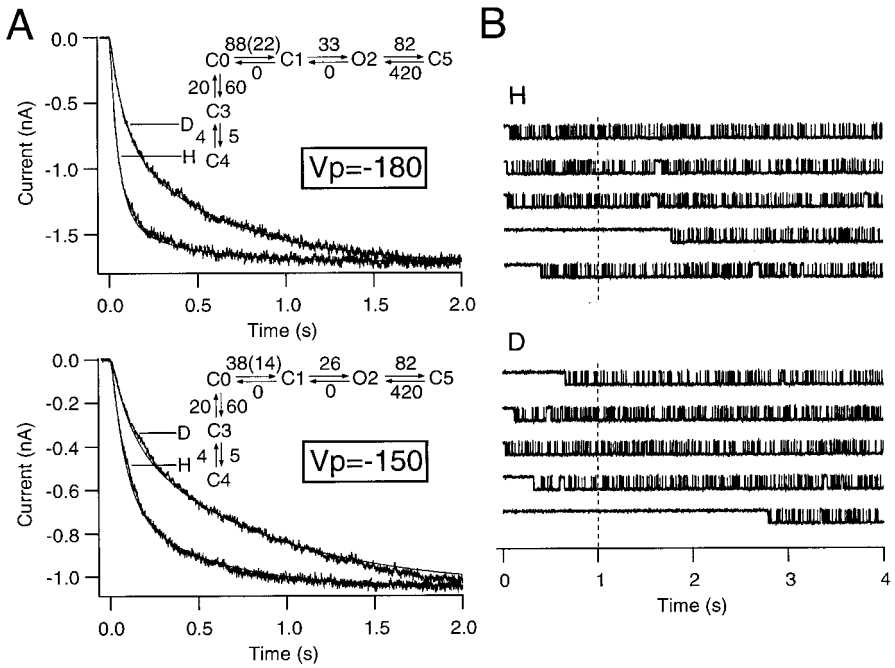

FIGURE 14 Scheme 4 predictions. (*A*) Macroscopic H118H and H118D currents simulated by Scheme 4. The values of the rate constants used in this simulation are shown. Different combinations of the rate constant values (k_{03}: 50–90 s^{-1}, k_{30}: 10–50 s^{-1}, k_{34}: 2–10 s^{-1}, and k_{43}: 2–10 s^{-1}) were manually tried to match the measured data. At time $t = 0$, all the channels were assumed to be in C0. The KAT1 current sweeps recorded at −180 mV (*upper panel*) and −150 mV (*lower panel*) were also shown superimposed. At each voltage examined, the single-channel amplitude was adjusted to fit the steady-state macroscopic current amplitude. (*B*) Single-channel H118H and H118D currents simulated by Scheme 4. The rate constants in upper panel of (*A*) are used. Note the prolonged first latency for H118H (fourth sweep in *upper panel*). If the pulse duration is shorter (e.g., 1 s), the fourth sweep in the upper panel and fifth sweep in the lower panel will be recorded as blank (null) sweeps. The first latency events for the H118D channel are even longer (*lower panel*; also see Fig. 10 *A* for the latency difference between the recorded H118H and H118D currents). However, after the channel opens, the steady-state single-channel kinetics is similar in H118H and H118D. The single channel conductance was set at 6 pS and the RMS noise of 0.1 pA was added to the simulated outputs.

match the measured results, including some prolonged first latency events in H118D. We also found that the accelerated activation time course in the H118K channel could also be simulated by increasing the value of $k_{01(0)}$ by ~190% without a change in its voltage dependence ($n = 3$, data not shown).

In Scheme 4, C0, C1, O2, and C5 are required to describe the activation kinetics and the fast single-channel closures. These states are well constrained by the experimental results. C4 and C3, which sequentially communicated with C0, are responsible for the slow activation component. How C4 and C3 communicate with the remaining states (C0, C1, O2, C5) is less constrained in part because our ionic currents measurements are well suited for the states near the open state, and those that are further away from the open state are more difficult to study. For example, C4 and C3 could communicate directly and separately with C0, generating a branched scheme. Simulation using this branched scheme indicates that this model may also successfully simulate the results (data not shown). However, we considered Scheme 4, a linear scheme, to be conceptually simpler than this branched model and adopted Scheme 4 as the final model in this study.

DISCUSSION

Stomatal opening, K_H channels and pH

The rhythmic openings and closures of stomata (Stålfelt, 1965) are regulated by light, CO_2 level, and humidity (Raschke, 1979; Irving et al., 1991; Assmann, 1996). Intracellular and extracellular pH and hyperpolarization-activated K^+ channels play pivotal roles in the stomatal opening process. The rhythmic movements of stomata are accompanied by oscillations in pH_i induced by an increased malic acid synthesis (Irving et al., 1991). An increase in pH_i activates electrogenic H^+-pumps in the guard cell membrane, causing hyperpolarization to a level more negative than the reversal potential of K^+-selective channels (E_K). The resting potential of the guard cell is reported to be as negative as about −250 mV when bathed in a solution with a millimolar K^+ outside (Thiel et al., 1992). At these extreme negative voltages, extracellular K^+ ions are driven into the guard cells through $GCKC1_{in}$. This K^+ uptake coupled with Cl^- uptake or an increase in malate anions increases the cytosolic osmotic pressure, resulting in guard cell swelling and water influx.

$GCKC1_{in}$, KAT1, and KST1 are up-regulated by protons from both the extra- and intracellular sides so that the channels open faster and more channels are open when pH decreases (Blatt, 1992; Hedrich et al., 1995; Hoshi, 1995; Müller-Röber et al., 1995; Grabov and Blatt, 1997; Hoth et al., 1997; Dietrich et al., 1998; Roelfsema and Prins, 1998; Brüggemann et al., 1999a; Hoth and Hedrich, 1999). This pH regulation is physiologically relevant because both extracellular and intracellular pH are known to change during the stomatal movements (Irving et al., 1991; Edwards et al., 1994). Extracellular pH varies between 7.2 and 5.1 during stomatal opening (Edwards et al., 1994). A decreased pH_i before stomatal opening was also observed in guard cells of the orchid *Paphiopedilum tonsum* (Irving et al., 1991). These changes in pH_i and pH_o are expected to affect $GCKC1_{in}$, which, in turn, affects the guard cell action potentials (Mummert and Gradmann, 1991; Thiel et al., 1992; Gradmann et al., 1993; Roelfsema and Prins, 1998). Oscillations in the plant cell membrane potential play a crucial role in the osmotic adjustments (Gradmann et al., 1993) that underlie stomatal activity, leaf movement, and plant growth (Schroeder et al., 1994). Changes in the activation kinetics of $GCKC1_{in}$ are expected to noticeably affect the amplitude and frequency of the guard-cell action potential. A simulation study suggests that even small changes in ion channel kinetics may result in profound changes in the plant cell membrane potential oscillation (Mummert and Gradmann, 1991; Gradmann et al., 1993).

Biophysical mechanism underlying the channel regulation by histidine-118

The mutations of H118 in the S2–S3 linker segment, which is thought to face the cytoplasmic side (Uozumi et al., 1998), specifically control the activation process of the KAT1 channel expressed in *Xenopus* oocytes. The results presented in this study are consistent with the idea that protonation and deprotonation of H118 play an important role in regulation of KAT1 T_A by pH_i. The following observations suggest that the amino acid at position 118 interacts with its effector site(s) through electrostatic interactions. K and R, with chemically very different side chains (Richardson and Richardson, 1989), produce similar acceleration. E and D produce similar slowing of the activation kinetics. A and N do not cause any obvious change in T_A.

KST1 has a glutamate at the H118-equivalent position, and its T_A is similar to that of KAT1 H118E or H118D. Together with the fact that $GCKC1_{in}$ differs markedly in its activation kinetics among various plant species (Fairley-Grenot and Assmann, 1993; Hedrich and Dietrich, 1996; Dietrich et al., 1998; Brüggemann et al., 1999b), it is likely that $GCKC1_{in}$ in different plants may have different amino acids at the KAT1 H118-equivalent positions. If that is the case, the quantitative difference in pH_i regulation of the KAT1 channel expressed in oocytes and the native $GCKC1_{in}$ (Fig. 5; also see Dietrich et al., 1998) could be caused by formation of heteromultimeric channels involving different α-subunits in native plant cells (cf. Dreyer et al., 1997). It is also possible that β subunits (Tang et al., 1996) may contribute to regulation of the activation kinetics.

Intracellular pH_i sensors have other components

Our results suggest that histidine at position 118 in the S2–S3 linker segment mediates the effect of low pH_i on T_A. Substitution of H118 with other amino acids largely but not completely eliminates the pH_i dependence of the activation kinetics in the pH range between 6 and 8. However, H118 alone does not account for all the observed effects of pH_i on the KAT1 channel (Hoshi, 1995). For example, lowering pH_i not only accelerates T_A but also slows T_{DA} at a given voltage, thus dramatically shifting the macroscopic $G(V)$ curve to a more positive direction (Hoshi, 1995). The H118 mutations, however, do not alter T_{DA} or the steady state $G(V)$. Thus, the H118 mutations alone do not account for the slowing of T_{DA} of wildtype KAT1 channel by lowering pH_i. Furthermore, the channels with uncharged amino acids at position 118 (A, N) still show small but noticeable pH_i sensitivity (Fig. 7). This is unexpected considering that the channels with K, R, E, or D at this position do not show much pH_i dependence in the same range, and, currently, there is no clear explanation. The residual pH sensitivity is much less steep than that predicted by the simple Henderson–Hasselbalch formulation. Multiple H^+ binding sites on a single KAT1 channel, with cooperativity among them, could produce such shallow pH dependence.

The single-channel analysis, which is well suited to analyze the transitions near the open state, indicates that the gating properties of the KAT1 channel are not obviously affected by the H118 mutations. The mean open and closed durations were essentially unaltered by the mutations. This specificity of the H118 mutation is reminiscent of the specific effect of the KAT1 rundown mediated by PKA-mediated phosphorylation and dephosphorylation (Tang and Hoshi, 1999). PKA-mediated phosphorylation, either directly or indirectly, alters only the opening transitions of the KAT1 channel before opening without affecting the channel properties after it opens. It is thus possible that histidine-118 and phosphorylation may affect the same effector site(s).

Gating model for the KAT1 channel activation

Based on the single-channel analysis, the activation time course of KAT1 activation was modeled by a linear scheme with one open state, a short-lived closed state after the open state, and three sequential closed states before the open state (Zei and Aldrich, 1998). This model successfully accounts for the main gating properties of the wildtype KAT1 channel and its S4 mutants. The late slow phase of the macro-

scopic currents and the blank sweeps seen in some first latency distributions were out of the scope of their model. We found that the slow activation component is readily observed in the macroscopic activation time course. More importantly, it is enhanced in the H118D (Figs. 5 and 14) and H118E channels (Fig. 5). As suggested by Zei and Aldrich (1998), additional closed states branching from the closed states in their linear scheme were necessary to account for the slow component. We find that two more closed states are necessary to simulate KAT1 T_A including the slow component (Fig. 14). Furthermore, changes in the value of one forward rate constant at 0 mV without affecting its voltage dependence could simulate the effects of the H118 mutations on T_A in the voltage range where the opening rate constants dominate. A positively charged residue at position 118 increases the rate constant value by about 190% (data not shown) and a negatively charged residue decreases the rate constant value by ~65% (Fig. 14). The proposed model adequately accounts for the changes in T_A caused by the H118 mutations at the voltages where the open probability is nearly saturated. However, the model's applicability to more positive voltages where the closing transition rate constants are no longer negligible was out of the current modeling scope and remains uncertain.

In summary, we have shown that histidine-118 in the putative cytoplasmic S2–S3 linker specifically affects T_A and contributes in part to the pH_i dependence of KAT1 expressed in oocytes. Activation time course of the wildtype KAT1 and various H118 mutant channels can be modeled by adjusting the value of a single rate constant in a sequential linear scheme. These results provide a molecular and biophysical basis for the diversity in the activation kinetics of inward rectifiers among different plant species, which may reflect evolutionary adaptation for plants to survive in diverse environmental conditions.

We thank Dr. Thommandru and Ms. Masropour for technical assistance, Dr. V. Avdonin for comments on the manuscript, and J. Bruce for the time sequence data.

This work was supported in part by National Institutes of Health (GM51474 to TH) and by Deutsche Forschungsgemeinschaft to RH.

REFERENCES

Anderson, J. A., S. S. Huprikar, L. V. Kochian, W. J. Lucas, and R. F. Gaber. 1992. Functional expression of a probable *Arabidopsis thaliana* potassium channel in *Saccharomyces cerevisiae*. *Proc. Natl. Acad. Sci. USA.* 89:3736–3740.

Assmann, S. M. 1996. Guard cell G proteins. *Trend. Plant Sci.* 1:73–74.

Avdonin, V., E. Shibata, and T. Hoshi. 1997. Dihydropyridine action on voltage-dependent potassium channels expressed in *Xenopus* oocytes. *J. Gen. Physiol.* 109:169–180.

Blatt, M. R. 1992. K^+ channels of stomatal guard cells: characteristics of the inward rectifier and its control by pH. *J. Gen. Physiol.* 99:615–644.

Blatt, M. R. 1997. Plant potassium channels double up. *Trend. Plant Sci.* 2:244–246.

Blatt, M. R., and G. Thiel. 1994. K^+ channels of stomatal guard-cells: bimodal control of the K^+ inward-rectifier evoked by auxin. *Plant J.* 5:55–68.

Brüggemann, L., P. Dietrich, D. Becker, I. Dreyer, K. Palme, and R. Hedrich. 1999a. Channel-mediated high-affinity K^+ uptake into guard cells from *Arabidopsis. Proc. Natl. Acad. Sci. USA.* 96:3298–3302.

Brüggemann, L., P. Dietrich, I. Dreyer, and R. Hedrich. 1999b. Pronounced differences between the native K^+ channels and KAT1 and KST1 α-subunit homomers of guard cells. *Planta.* 207:370–376.

Butt, A. D., M. R. Blatt, and C. C. Anisworth. 1997. Expression, evolution and genomic complexity of potassium ion channel genes of *Arabidopsis thaliana. Plant Physiol. (Rockville).* 150:652–660.

Cao, Y., J. M. Ward, W. B. Kelly, A. M. Ichida, R. F. Gaber, J. A. Anderson, N. Uozumi, J. I. Schroeder, and N. M. Crawford. 1995. Multiple genes, tissue specificity, and expression-dependent modulation contribute to the functional diversity of potassium channels in *Arabidopsis thaliana. Plant Physiol. (Rockville).* 109:1093–1106.

Coulter, K. L., F. Perier, C. M. Radeke, and C. A. Vandenberg. 1995. Identification and molecular localization of a pH-sensing domain for the inward rectifier potassium channel HIR. *Neuron.* 15:1157–1168.

Dietrich, P., I. Dreyer, P. Wiesner, and R. Hedrich. 1998. Cation sensitivity and kinetics of guard-cell potassium channels differ among species. *Planta.* 205:277–287.

Dreyer, I., S. Antunes, T. Hoshi, B. Müller-Röber, K. Palme, O. Pongs, B. Reintanz, and R. Hedrich. 1997. Plant K^+ channel alpha-subunits assemble indiscriminately. *Biophys. J.* 72:2143–2150.

Edsall, J. T., and J. Wyman. 1958. Biophysical Chemistry. Academic Press, New York.

Edwards, M. C., G. N. Smith, and D. J. F. Bowling. 1994. Guard cells extrude protons prior to stomatal opening: A study using fluorescence microscopy and pH micro-electrode. *J. Exp. Bot.* 39:1541–1547.

Ehrhardt, T., S. Zimmermann, and B. Müller-Röber. 1997. Association of plant K^+ in channel is mediated by conserved C-termini and does not affect channel assembly. *FEBS Lett.* 409:166–170.

Fairley-Grenot, K. A., and S. M. Assmann. 1993. Comparison of K^+-channel activation and deactivation in guard cells from a dicotyledon (*Vicia faba* L.) and a graminaceous monocotyledon (*Zea mays*). *Planta.* 189:410–419.

Fakler, B., J. H. Schultz, J. Yang, U. Schulte, U. Brändle, H. P. Zenner, L. Y. Jan, and J. P. Ruppersberg. 1996. Identification of a titratable lysine residue that determines sensitivity of kidney potassium channels (ROMK) to intracellular pH. *EMBO J.* 15:4093–4099.

Fischer, R. A. 1968. Stomatal opening: role of potassium uptake by guard cells. *Science.* 160:784–785.

Grabov, A., and M. R. Blatt. 1997. Parallel control of the inward-rectifier K^+ channels by cytosolic free Ca^{2+} and pH in *Vicia* guard cells. *Planta.* 201:84–95.

Gradmann, D., M. R. Blatt, and G. Thiel. 1993. Electrocoupling of ion transporters in plants. *J. Membr. Biol.* 136:327–332.

Hedrich, R., H. Busch, and K. Raschke. 1990. Ca^{2+} and nucleotide dependent regulation of voltage dependent anion channels in the plasma membrane of guard cells. *EMBO J.* 9:3889–3892.

Hedrich, R., and P. Dietrich. 1996. Plant K^+ channels: similarity and diversity. *Bot. Acta.* 109:94–101.

Hedrich, R., O. Moran, F. Conti, H. Busch, D. Becker, F. Gambale, I. Dreyer, A. Kuech, K. Neuwinger, and K. Palme. 1995. Inward rectifier potassium channels in plants differ from their animal counterparts in response to voltage and channel modulators. *Eur. Biophys. J.* 24: 107–115.

Hille, B. 1992. Ionic Channels of Excitable Membranes. Sinauer Associates, Inc., Sunderland, MA.

Hirsch, R. E., B. D. Lewis, E. P. Spalding, and M. R. Sussman. 1998. A role for the AKT1 potassium channel in plant nutrition. *Science.* 280: 918–921.

Hoshi, T. 1995. Regulation of voltage dependence of the KAT1 channel by intracellular factors. *J. Gen. Physiol.* 105:309–328.

Hoshi, T., W. N. Zagotta, and R. W. Aldrich. 1990. Biophysical and molecular mechanisms of *Shaker* potassium channel inactivation. *Science.* 250:533–538.

Hoth, S., I. Dreyer, P. Dietrich, D. Becker, B. Müller-Röber, and R. Hedrich. 1997. Molecular basis of plant-specific acid activation of K^+ uptake channels. *Proc. Natl. Acad. Sci. USA.* 94:4806–4810.

Hoth, S., and R. Hedrich. 1999. Distinct molecular bases for pH sensitivity of the guard cell K^+ channels KST1 and KAT1. *J. Biol. Chem.* 274: 11599–11603.

Ilan, N., A. Schwartz, and N. Moran. 1994. External pH effects on the depolarization-activated K channels in guard cell protoplasts of *Vicia faba. J. Gen. Physiol.* 103:807–831.

Irving, H. R., C. A. Gehring, and A. W. Parish. 1991. Change in cytosolic pH and calcium of guard cells precede stomatal movements. *Proc. Natl. Acad. Sci. USA.* 89:1790–1794.

Ketchum, K. A., and C. W. Slayman. 1996. Isolation of an ion channel gene from *Arabidopsis thaliana* using the H5 signature sequence from voltage-dependent K^+ channels. *FEBS Lett.* 378:19–26.

Lagarde, D., M. Basset, M. Lepetit, G. Conejero, F. Gaymard, S. Astruc, and C. Grignon. 1996. Tissue-specific expression of *Arabidopsis* AKT1 gene is consistent with a role in K^+ nutrition. *Plant J.* 9:195–203.

López-Barneo, J., T. Hoshi, S. H. Heinemann, and R. W. Aldrich. 1993. Effects of external cations and mutations in the pore region on C-type inactivation of *Shaker* potassium channels. *Recept. Channels.* 1:61–71.

Marten, I., and T. Hoshi. 1997. Voltage-dependent gating characteristics of the K^+ channel KAT1 depend on the N- and C-termini. *Proc. Natl. Acad. Sci. USA.* 94:3448–3453.

Marten, I., and T. Hoshi. 1998. The N-terminus of the K^+ channel KAT1 controls its voltage-dependent gating by altering the membrane electric field. *Biophys. J.* 74:2953–2962.

Müller-Röber, B., J. Ellenberg, N. Provart, L. Willmitzer, H. Busch, D. Becker, P. Dietrich, S. Hoth, and R. Hedrich. 1995. Cloning and electrophysiological analysis of KST1, an inward rectifying K^+ channel expressed in potato guard cells. *EMBO J.* 14:2409–2416.

Mummert, H., and D. Gradmann. 1991. Action potentials in *Acetabularia*: measurement and simulation of voltage-gated fluxes. *J. Membr. Biol.* 124:265–273.

Nakamura, R. L., W. L. J. McKendree, R. E. Hirsch, J. C. Sedbrook, R. F. Gaber, and M. R. Sussman. 1995. Expression of an *Arabidopsis* potassium channel gene in guard cells. *Plant Physiol. (Rockville).* 109: 371–374.

Neher, E. 1992. Correction for liquid junction potentials in patch clamp experiments. *Methods Enzymol.* 207:123–131.

Raschke, K. 1979. Movement of stomata. *In* Plant Physiology (New Series 7). W. Haupt, and M. E. Feinleib, editors. Springer-verlag, Berlin, Heidelberg, New York. 383–441.

Richardson, J. S., and D. C. Richardson. 1989. Principles and patterns of protein conformation. *In* Prediction of Protein Structure and the Principles of Protein Conformation. G. D. Fasman, editor. Plenum, New York. 1–98.

Roelfsema, M. R. G., and H. B. A. Prins. 1998. The membrane potential of *Arabidopsis thaliana* guard cells: depolarization induced by apoplastic acidification. *Planta.* 205:100–112.

Schroeder, J. I., J. M. Ward, and W. Gassmann. 1994. Perspectives on the physiology and structure of inward rectifying K^+ channels in higher plants: biophysical implications for K^+ uptake. *Annu. Rev. Biophys. Biomol. Struct.* 23:441–471.

Sentenac, H., N. Bonneaud, M. Minet, F. Lacroute, J. M. Salmon, F. Gaymard, and C. Grignon. 1992. Cloning and expression in yeast of a plant potassium ion transport system. *Science.* 256:663–665.

Stålfelt, M. G. 1965. The relation between the endogenous and induced elements of the stomatal movements. *Physiol. Plant.* 18:177–184.

Tang, H., A. C. Vasconcelos, and G. A. Berkowitz. 1996. Physical association of KAB1 with plant K^+ channel alpha subunits. *Plant Cell.* 8:1545–1553.

Tang, X. D., and T. Hoshi. 1999. Rundown of the hyperpolarization-activated KAT1 channel involves slowing of the opening transitions regulated by phosphorylation. *Biophys. J.* 76:3089–3098.

Thiel, G., E. A. C. MacRobbie, and M. R. Blatt. 1992. Membrane transport in stomatal guard cells: The importance of voltage control. *J. Membr. Biol.* 126:1–18.

Uozumi, N., T. Nakamura, J. I. Schroeder, and S. Muto. 1998. Determination of transmembrane topology of an inward-rectifying potassium channel from *Arabidopsis thaliana* based on functional expression in *Escherichia coli. Proc. Natl. Acad. Sci. USA.* 95:9773–9778.

Zei, P. C., and R. W. Aldrich. 1998. Voltage-dependent gating of single wild-type and S4 mutant KAT1 inward rectifier potassium channels. *J. Gen. Physiol.* 112:679–713.

Zimmermann, S., I. Talke, T. Ehrhardt, G. Nast, and B. Müller-Röber. 1998. Characterization of SKT1, an inwardly rectifying potassium channel from potato, by heterologous expression in insect cells. *Plant Physiol. (Rockville).* 116:879–890.